Appearance-Based Face Recognition and Light-Fields

Ralph Gross, Iain Matthews, and Simon Baker

CMU-RI-TR-02-20

Abstract

Arguably the most important decision to be made when developing an object recognition algorithm is selecting the scene measurements or *features* on which to base the algorithm. In appearance-based object recognition the features are chosen to be the pixel intensity values in an image of the object. These pixel intensities correspond directly to the radiance of light emitted from the object along certain rays in space. The set of all such radiance values over all possible rays is known as the *plenoptic function* or *light-field*. In this paper we develop the theory of appearance-based object recognition from light-fields. This theory leads directly to a pose-invariant face recognition algorithm that uses as many images of the face as are available, from one upwards. All of the pixels, whichever image they come from, are treated equally and used to estimate the (eigen) light-field of the object. The *eigen light-field* is then used as the set of features on which to base recognition, analogously to how the pixel intensities are used in appearance-based object recognition. We also show how our algorithm can be extended to recognize faces across pose and illumination by using *Fisher light-fields.*

1 Introduction

Arguably the most important decision to be made when developing an object recognition algorithm is selecting the scene measurements or *features* on which to base the algorithm. One of the most successful and well-studied approaches to object recognition is the *appearance-based* approach. Although the expression "appearance-based" was introduced by Murase and Nayar [17], the approach itself dates back to Turk and Pentland's *Eigenfaces* [25] and perhaps before [24]. The defining characteristic of appearance-based algorithms is that they directly use the pixel intensity values in an image of the object as the features on which to base the recognition decision.

The pixel intensities that are used as features in appearance-based algorithms correspond directly to the radiance of light emitted from the object along certain rays in space. Although there may be various non-linearities caused by the optics (e.g. vignetting), the CCD sensor itself, or by gamma correction in the camera, the pixel intensities can be thought of as approximately equivalent to the radiance of light emitted from the object in the direction of the pixel.

The *plenoptic function* [1] or *light-field* [12, 16] specifies the radiance of light along all rays in the scene. Hence, the light-field of an object is the set of all possible features that could be used by an appearance-based object recognition algorithm. It is natural, therefore, to investigate using light-fields (as an intermediate representation) for appearance-based object recognition. In the first part of this paper we develop the theory of appearance-based object recognition from light-fields. In the second part we propose an algorithm for pose-invariant face recognition based on an algorithm to estimate the (eigen) light-field of a face from a set of images. Finally, we extend our algorithm to perform face recognition across both pose and illumination using Fisher light-fields.

1.1 Theoretical Properties of Light-Fields for Recognition

There are a number of important theoretical questions pertaining to object recognition from light-fields. Some examples are:

1. The fundamental question "what is the set of images of an object under all possible illumination conditions?" was recently posed and answered in [5]. Because an image simply consists of a subset of measurements from the light-field, it is natural to ask the same question about the set of all light-fields of an object. Answering this second question may also help understand the variation in appearance of objects across both pose and illumination.

2. "When can two objects be distinguished from their images?" is perhaps the most important theoretical question in object recognition. Various attempts have been made to answer it in one form or another. For example, it was shown in [4] that, given a pair of images, there is always an object that could have generated those two images (under different illuminations.) Similarly one might ask "when can two objects be distinguished from their light-fields?"

In the first part of this paper we derive a number of fundamental properties of object light-fields. In particular, we first investigate the set of all possible light-fields of an object under varying illumination. Amongst other things we show that the set of all light-fields is a convex cone, analogously to the results in [5] for single images. Afterwards we investigate the degree to which objects are distinguishable from their light-fields. We show that, under arbitrary illumination conditions, if two objects have the same shape they cannot be distinguished, even given their light-field. The situation for objects with different shapes is different however. We show that two objects can almost always be distinguished from their light-fields if they have different shapes.

1.2 Face Recognition Using Light-Fields

One implication of this theory is that "appearance-based" object recognition from light-fields is theoretically more powerful than object recognition from single images. Capturing an entire light-field is normally not appropriate for object recognition however; it requires either a large number of cameras, a great deal of time, or both. This does not mean that it is impossible to use light-fields in practical object recognition algorithms. In the second part of this paper we develop a pose-invariant face recognition algorithm that is based on an algorithm to estimate the (eigen) light-field

of an object from an arbitrary collection of images [13]. This algorithm is based on an algorithm for dealing with occlusions in the eigen-space approach [6, 15]. The eigen light-field, once it has been estimated, is then used as an enlarged set of features on which to base the face recognition decision. Some of the advantageous properties of this algorithm are as follows:

1. Any number of images can be used, from one upwards, in both the training (gallery) and the test (probe) sets. Moreover, none of the training images need to have been captured from the same pose as any of the test images. For example, there might be two test images for each person, a full frontal view and a full profile, and only one training image, a half profile. In this way, our algorithm can perform "face recognition across pose."

2. If only one test or training image is available, our algorithm behaves "reasonably" when estimating the light-field. In particular, we prove that the light-field estimated by our algorithm correctly re-renders images across pose (under suitable assumptions about the objects.)

3. If more than one test or training image is available, the extra information (including the implicit shape information) is incorporated into a better estimate of the light-field. The final face recognition algorithm therefore performs demonstrably better with more input images.

4. It is straightforward to extend our algorithm to perform "face recognition across both pose and illumination" [14]. We generalize *eigen light-fields* to *Fisher Light-fields* analogously to how eigenfaces were generalized to Fisherfaces in [3].

1.3 Overview

The remainder of this paper is organized as follows. We begin in Section 2 by introducing object light-fields and deriving some of their key properties. We continue in Section 3 by describing eigen light-fields and their use in our algorithm for face recognition across pose. In Section 4 we extend our algorithm to use Fisher light-fields and to recognize faces across both pose and illumination. We conclude in Section 5 with a summary and suggestions for future work.

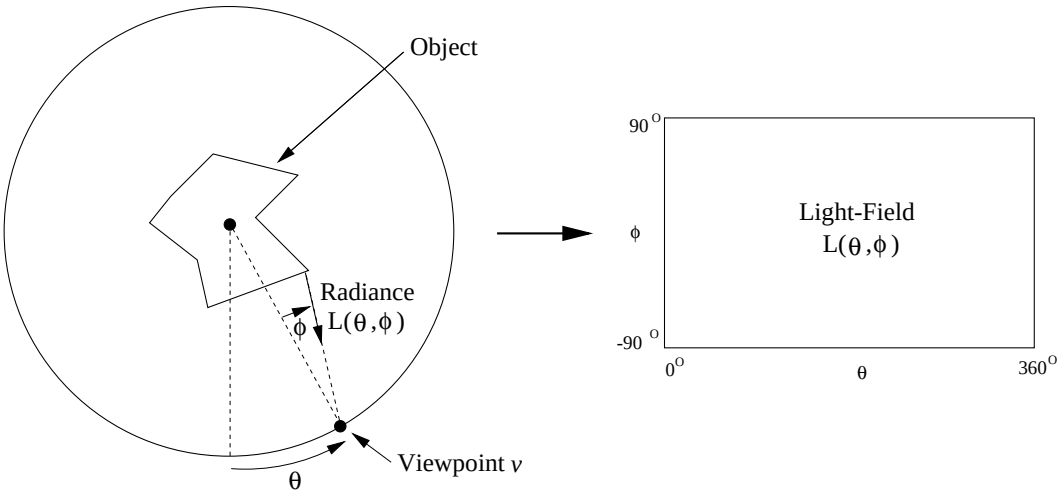

Figure 1: An illustration of the 2D light-field [16] of a 2D object. The object is conceptually placed within a circle. The angle to the viewpoint v around the circle is measured by the angle θ and the direction that the viewing ray makes with the radius of the circle by ϕ. For each pair of angles θ and ϕ, the radiance of light reaching the viewpoint is denoted $L(\theta, \phi)$, the *light-field* [16]. Although the light-field of a 3D object is actually 4D, we will continue to use the 2D notation of this figure for ease of explanation.

2 Object Light-Fields and Their Properties for Recognition

2.1 Object Light-Fields

The *plenoptic function* [1] or *light-field* [16] is a function which specifies the radiance of light in free space. It is usually assumed to be a 5D function of position (3D) and orientation (2D). In addition, it is also sometimes modeled as a function of time, wavelength, and polarization, depending on the application in mind. Assuming that there is no absorption or scattering of light through the air [18], the light-field is actually only a 4D function, a 2D function of position defined over a 2D surface, and a 2D function of direction [12, 16]. In 2D, the light-field of a 2D object is only 2D. See Figure 1 for an illustration of the 2D light-field of a 2D object.

2.2 The Set of All Light-Fields of an Object Under Varying Illumination

The fundamental question "what is the set of images of an object under all possible illumination conditions?" was recently posed and answered by Belhumeur and Kriegman [5]. We begin our analysis by asking the analogous question for light-fields. Since an image just consists of a subset of the rays in the light-field, it is not surprising that the same result also holds for light-fields:

Theorem 1 *The set of n-pixel* light-fields *of any object, seen under all possible lighting conditions, is a convex cone in* $\mathbf{R}^n$.

This result holds for any object, even if the object is non-convex and non-Lambertian. As pointed out in [5], the proof is essentially a trivial combination of the additive property of light and the fact that the set of *all* illumination conditions is itself a *convex cone.* For this reason, the same result holds for any subset of illumination conditions that is a convex cone. One example is an arbitrary number of point light sources at infinity. It is straightforward to show that this subset of illumination conditions is a convex cone and therefore that the following theorem also holds:

Theorem 2 *The set of n-pixel* light-fields *of any object, illuminated by an arbitrary number of point light sources at infinity, is a convex cone in* $\mathbf{R}^n$.

These results are analogous to those in [5]. Moreover, since Theorems 1 and 2 clearly also hold for any subset of rays in the light-field, the analogous results in [5] are special cases of these theorems.

When we investigate the nature of the illumination cones in more detail, however, we find several differences between images and light-fields. Some of the differences are summarized in Table 1. If we consider arbitrary illumination conditions and any convex object, the image illumination cone *always exactly equals the set of all images* because every point on the object can be illuminated independently and set to radiate any intensity. This result holds for any reflectance function. The only minor requirement is that no point on the object has zero reflectance.

The situation is different for light-fields. It is possible to choose reflectance functions for which the light-field illumination cone is equal to the set of all light-fields. One simple example

Table 1: A comparison of image illumination cones and light-field illumination cones. The main point to note is that in three of the four cases, the light-field illumination cone is a "smaller" subset of the set of all light-fields than the corresponding image illumination cone is a subset of the set of all images.

	Image Illumination Cone	Light-field Illumination Cone
Arbitrary Illumination Conditions Any Convex Object	*Always exactly equals* the set of all images	*Can sometimes be* the set of all light-fields
Arbitrary Illumination Conditions Convex Lambertian Object	*Always exactly equals* the set of all images	*Never is* the set of all light-fields
Point Light Sources at Infinity Any Convex Object	*Can sometimes be* full-dimensional	*Can sometimes be* full-dimensional
Point Light Sources at Infinity Convex Lambertian Object	*Can sometimes be* full-dimensional	*Never is* full-dimensional

is to use a "mirrored" object. However, for most reflectance functions the light-field illumination cone is *not equal* to the set of all light-fields. One example is Lambertian reflectance. In this case, the light-field cone *never equals* the set of all light-fields because any two pixels in the light-field that image the same point on the object will always have the same intensity. For Lambertian objects the image illumination cone across arbitrary illumination conditions still *exactly equals* the set of all images because the pixels can still all be set independently by choosing the illumination appropriately.

For point light sources at infinity (rather than for arbitrary illumination conditions), the results are similar. The image illumination cone can sometimes be full-dimensional. For convex Lambertian objects the dimensionality equals the number of distinct surface normals. (See [5] Proposition 5.) If each surface normal is different, the image illumination cone is full-dimensional. For light-fields, however, the light-field illumination cone of a convex Lambertian object with point light sources at infinity is never full dimensional because any two pixels in the light-field that image the same point on the surface will always have the same intensity.

The trend in Table 1 is clear. Object recognition in the presence of illumination changes is "theoretically" easier using light-fields than with images. Using either model (arbitrary illumination or point light sources at infinity) the light-field illumination cone is a "smaller" subset of the set of all light-fields than the image illumination cone is a subset of the set of all images.

2.3 Distinguishability of Objects from Their Images and Light-Fields

As mentioned in [5] the convex cone property is potentially very important for object recognition because it implies that if the illumination cones of two objects are disjoint, they can be separated by a linear discriminant function. This property makes classification much easier because applying a linear classifier is in general far easier than determining which illumination cone an image or light-field lies closest to. However, to take advantage of this property, the two illumination cones must be disjoint. If they are not the two objects will not always be distinguishable anyway. These arguments, of course, apply equally to both image and light-field illumination cones. In this section we study the distinguishability (intersection) of illumination cones and show that the task is theoretically easier for light-fields than for images. We begin with image illumination cones.

2.3.1 Distinguishability of Objects from Their Images

An immediate corollary of the fact that the image illumination cones of convex objects under arbitrary lighting are exactly equal to the set of all images (see Table 1) is that no two convex objects (Lambertian or not) can *ever* be distinguished without some assumptions about the illumination:

Corollary 1 *The image illumination cones of any two convex objects seen under all possible lighting conditions are exactly equal. It is therefore never possible to say which convex object an image came from. It is not even possible to eliminate any convex objects as possibilities.*

Perhaps one of the most important results of [5] is to show that, if the illumination consists of point sources at infinity the situation is more favorable; empirically the volume of the image illumination

cone is much less than the space of all images. It is also straight-forward to show that there are pairs of objects that are distinguishable under this smaller set of lighting conditions:

Theorem 3 *There exist pairs of objects for which the intersection of their illumination cones (over the set of illumination conditions consisting of arbitrary numbers of point light sources at infinity) only consists of the black (all zero) image; i.e. there are pairs of objects that are always distinguishable (over the set of illumination conditions which consist of point light sources at infinity.)*

Proof: (Sketch) One example is to consider two Lambertian spheres, one with an albedo function that has multiple step discontinuities (which appear in every image), one that varies smoothly everywhere. All of the images of the object with the step discontinuity in the albedo map will also have a step discontinuity in the image, whereas none of the images of the other object will. □

Although we have shown that there are pairs of objects for which the image illumination cones (for point light sources at infinity) only intersect at the all black image, there are pairs of objects for which their image illumination cones do intersect.

Theorem 4 *There exist pairs of objects for which the intersection of their illumination cones (over the set of point light sources at infinity) consists of more than just the black (all zero) image; i.e. there are pairs of objects that are sometime indistinguishable (over point light sources at infinity.)*

Proof: Consider two convex Lambertian objects in different illuminations. If each object has albedo variation proportional to the foreshortened incoming illumination of the other object, the two objects will generate the same image. (The constants of proportionality must be the same.) □

2.3.2 Distinguishability of Same-Shape Objects from Their Light-Fields

In the previous section we showed that distinguishing objects from their images under varying illumination is often very difficult, and in many cases “theoretically” impossible. If the objects are the same shape, convex, and Lambertian, intuitively the light-field should not contain any

additional information. It is no surprise, then, that it is fairly straight-forward to prove an analogy of Corollary 1 for (convex Lambertian) objects of the same shape:

Theorem 5 *The light-field illumination cones over all possible lighting conditions of any two convex, Lambertian objects of the same shape are exactly equal.*

Proof: Given arbitrary lighting, it is possible to generate any incoming radiance distribution over the surface of the (convex) object using lasers. It is therefore possible to generate any light-field for any convex object (subject to the necessary and sufficient constraint that rays imaging the same point on the surface of the object have the same intensity.) □

Distinguishing (convex Lambertian) objects of the same shape from their light-fields is therefore impossible without any assumptions on the illumination. If assumptions are made about the illumination, the situation is different. As in Theorems 3 and 4 above, if the illumination consists of point light sources at infinity two objects of the same shape may or may not be distinguishable.

Theorem 6 *There exist pairs of same-shape convex, Lambertian objects for which the intersection of their light-field illumination cones (over the set of point light sources at infinity) only consists of the black (all zero) light-field; i.e. there are pairs of same-shape objects that are always distinguishable (over the set of point light sources at infinity.)*

Proof: Essentially the same as the proof of Theorem 3. □

Theorem 7 *There exist pairs of convex, Lambertian objects with the same shape for which the intersection of their light-field illumination cones (over the set of point light sources at infinity) consists of more than just the black (all zero) image; i.e. there are pairs of same-shape objects that are sometime indistinguishable even given their light-fields.*

Proof: Essentially the same as the proof of Theorem 4. □

2.3.3 Distinguishability of Differently-Shaped Objects from Their Light-Fields

Intuitively the situation for differently shaped objects is different. The light-field contains considerable information about the shape of the objects. In fact, we recently showed in [2] that, so long as the light-field does not contain any extended constant intensity regions, it uniquely defines the shape of a Lambertian object. This means that the intersection of the light-field cones of two differently shaped objects must only contain light-fields that have constant intensity regions.

Theorem 8 *The intersection of the light-field illumination cones over all possible lighting conditions of any two Lambertian objects that have different shapes only consists of light-fields that have constant intensity regions.*

This theorem implies that two differently shaped Lambertian objects can always be distinguished from any light-field that does not contain constant intensity regions.

2.3.4 Summary

We have described various conditions under which pairs of objects are distinguishable from their images or light-fields. See Table 2 for a summary. When nothing is assumed about the incoming illumination, it is impossible to distinguish between any pair of objects from their images. If the illumination consists of a collection of point light sources at infinity, the situation is a little better. Some pairs of objects can always be distinguished, but other pairs are sometimes indistinguishable.

If the objects have the same shape the situation is the same with light-fields. Light-field don't add to the discriminatory power of a single image. If the objects have different shapes the light-field adds a lot of discriminatory power. So long as the light-field has no constant intensity regions, any pair of differently shaped objects can be distinguished under any illumination conditions.

Table 2: The distinguishability of objects from their images and light-fields. The main point to note is that if two objects have the same shape, the light-field adds nothing to the ease with which they can be distinguished, compared to just a single image. On the other hand, if the two objects have different shapes, it is theoretically far easier to distinguish them from their light-fields than it is from single images.

	Arbitrary Illumination Conditions	Point Light Sources at Infinity
Images of Two Convex Lambertian Objects	Never Distinguishable (Corollary 1)	Sometimes Distinguishable (Thm. 3) Sometime Indistinguishable (Thm. 4)
Light-fields of Two Same Shape Convex Lambertian Objects	Never Distinguishable (Theorem 5)	Sometimes Distinguishable (Thm. 6) Sometime Indistinguishable (Thm. 7)
Light-fields of Two Differently Shaped Lambertian Objects	Distinguishable if No Constant Intensity (Thm. 8)	Always Distinguishable if No Constant Intensity (Thm. 8)

2.4 Implications

The implication of these theoretical results is as follows. The light-field provides considerable information about the shape of objects that can help distinguish between them in unknown, arbitrary illumination conditions under which they would be indistinguishable from single images. Although it is practically impossible to capture the entire light-field for most object recognition tasks, sometimes it may be possible to capture 2-3 images. Ideally we would like an object recognition algorithm that can use any subset of the light-field; a single image, a pair of images, multiple images, or even the entire light-field. Such an algorithm should be able to take advantage of the implicit shape information in the light-field. In the remainder of this paper we describe exactly such an algorithm, the first step of which is to estimate the light-field from the input image(s).

3 Eigen Light-Fields for Face Recognition Across Pose

In many face recognition application scenarios the *pose* of the probe and gallery images are different. The gallery image might be a frontal "mug-shot" and the probe might be a 3/4 view captured from a surveillance camera in the corner of the room. The number of gallery and probe images may also vary. The gallery may consist of a pair of images of each subject, perhaps a frontal mug-shot and full profile view, like the images typically captured by police departments. The probe may be a similar pair of images, a single 3/4 view, or even a collection of views from random poses.

Until recently face recognition across pose (i.e. when the gallery and probe have different poses) has received very little attention in the literature. Algorithms have been proposed which can recognize faces [19] or more general objects [17] at a variety of poses. Most of these algorithms require gallery images at every pose, however. Algorithms have been proposed which do generalize across pose, for example [11], but this algorithm computes 3D head models using a gallery containing a large number of images per subject captured with controlled illumination variation. It cannot be used with arbitrary galleries and probes. Note, however, that concurrent with this work there has been a growing interest in face recognition across pose. For example, Vetter *et al* have developed an algorithm based on fitting a 3D morphable model [8, 22].

In this section we propose an algorithm for face recognition across pose using light-fields. Our algorithm can use any number of gallery images captured at arbitrary poses, and any number of probe images also captured with arbitrary poses. A minimum of 1 gallery and 1 probe image are needed, but if more images are available the performance of our algorithm generally gets better.

Our algorithm operates by estimating (a representation of) the light-field of the subject's head. First, generic training data is used to compute an eigen-space of head light-fields, similar to the construction of eigen-faces [25]. Light-fields are simply used rather than images. Given a collection of gallery or probe images, the projection into the eigen-space is performed by setting up a least-squares problem and solving for the projection coefficients similarly to approaches used to deal with occlusions in the eigenspace approach [15, 6]. This simple linear algorithm can be

applied to any number of images, captured from any poses. Finally, matching is performed by comparing the probe and gallery light-fields using a nearest neighbor algorithm.

The remainder of this section is organized as follows. We begin in Section 3.1 by introducing the concept of *eigen light-fields* before presenting the algorithm to estimate them from a collection of images in Section 3.2. After describing some of the properties of this algorithm in Section 3.3, we the describe how the algorithm can be used to perform face recognition across pose in Section 3.4. Finally, we present experimental face recognition across pose results in Section 3.5.

3.1 Eigen Light-Fields

Suppose we are given a collection of light-fields $L_i(\theta, \phi)$ where $i = 1, \ldots, N$. See Figure 1 for the definition of this notation. If we perform an eigen-decomposition of these vectors using Principal Components Analysis (PCA), we obtain $d \leq N$ eigen light-fields $E_i(\theta, \phi)$ where $i = 1, \ldots, d$. Then, assuming that the eigen-space of light-fields is a good representation of the set of light-fields under consideration, we can approximate any light-field $L(\theta, \phi)$ as:

$$L(\theta, \phi) \approx \sum_{i=1}^{d} \lambda_i E_i(\theta, \phi) \tag{1}$$

where $\lambda_i = \langle L(\theta, \phi), E_i(\theta, \phi) \rangle$ is the inner (or dot) product between $L(\theta, \phi)$ and $E_i(\theta, \phi)$. This decomposition is analogous to that used in face and object recognition [25, 17]; it is just performed on the entire light-field rather than on single images. (The mean light-field can be included as a constant additive term in Equation (1) and subtracted from the light-field in the definition of λ_i if so preferred. There is very little difference in doing this however.)

3.2 Estimating Light-Fields from Images

Capturing the complete light-field of an object is a difficult task, primarily because it requires a huge number of images [12, 16]. In most object recognition scenarios it is unreasonable to expect more than a few images of the object; often just one. As shown in Figure 2, however, any image of

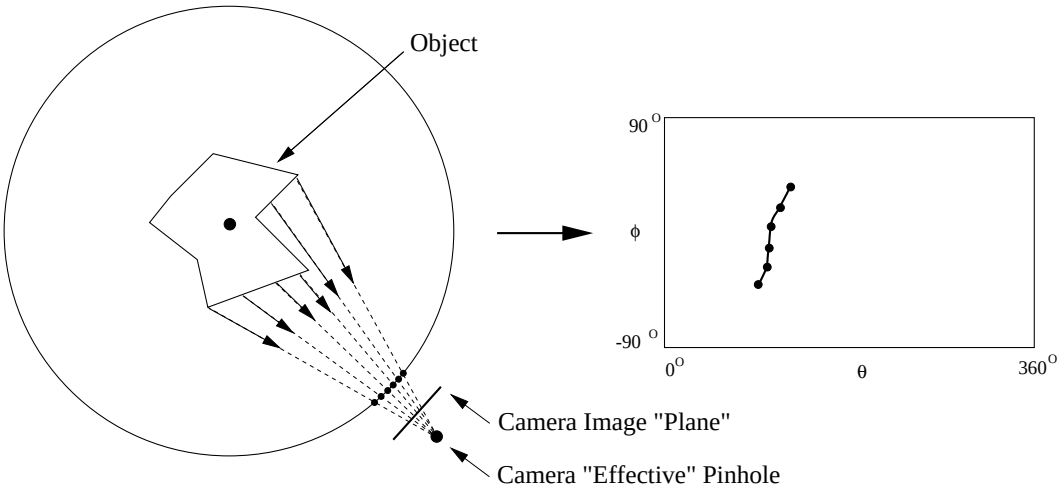

Figure 2: The 1D image of a 2D object corresponds to a curve (surface for a 2D image of a 3D object) in the light-field. Each pixel corresponds to a ray in space through the camera pinhole and the location of the pixel in the image. In general this ray intersects the light-field circle at a different point for each pixel. As the pixel considered "moves" in the image, the point on the light-field circle traces out a curve in θ-ϕ space. This curve is a straight vertical line iff the "effective pinhole" lies on the circle used to define the light-field.

the object corresponds to a curve (for 3D objects, a surface) in the light-field. One way to look at this curve is as a highly occluded light-field; only a very small part of the light-field is visible.

Can the coefficients λ_i be estimated from this highly occluded view? Although this may seem hopeless, note that light-fields are highly redundant, especially for objects with simple reflectance properties such as Lambertian. An algorithm is presented in [15] to solve for the unknown λ_i for eigen-*images*. A similar algorithm was used in [6]. Rather than using the inner product $\lambda_i = \langle L(\theta, \phi), E_i(\theta, \phi) \rangle$, Leonardis and Bischof [15] solve for λ_i as the least squares solution of:

$$L(\theta, \phi) - \sum_{i=1}^{d} \lambda_i E_i(\theta, \phi) \; = \; 0 \tag{2}$$

where there is one such equation for each pair of θ and ϕ that are un-occluded in $L(\theta, \phi)$. Assuming that $L(\theta, \phi)$ lies *completely within the eigen-space* and that enough pixels are un-occluded, then the solution of Equation (2) will be exactly the same as that obtained using the inner product:

Theorem 9 *Assuming that $L(\theta, \phi)$ is in the linear span of $\{E_i(\theta, \phi) \mid i = 1, \ldots d\}$, then $\lambda_i = \langle L(\theta, \phi), E_i(\theta, \phi) \rangle$ is always an exact minimum solution of Equation (2).*

Since there are d unknowns ($\lambda_1 \ldots \lambda_d$) in Equation (2), at least d un-occluded light-field pixels are needed to over-constrain the problem, but more may be required due to linear dependencies between the equations. In practice, $2 - 3$ times as many equations as unknowns are typically required to get a reasonable solution [15]. Given an image $I(m, n)$, the following is then an algorithm for estimating the eigen light-field coefficients λ_i:

Eigen Light-Field Estimation Algorithm

1. For each pixel (m, n) in $I(m, n)$ compute the corresponding light-field angles $\theta_{m,n}$ and $\phi_{m,n}$. (This step assumes that the camera intrinsics are known, as well as the relative orientation between the camera and object. In Section 3.4.1 we will describe how to avoid this step and instead use a simple "normalization" to convert the input images into light-field vectors.)
2. Find the least-squares solution (for $\lambda_1 \ldots \lambda_d$) to the set of equations:

$$I(m, n) - \sum_{i=1}^{d} \lambda_i E_i(\theta_{m,n}, \phi_{m,n}) \; = \; 0 \tag{3}$$

   where m and n range over their allowed values. (In general, the eigen light-fields E_i need to be interpolated to estimate $E_i(\theta_{m,n}, \phi_{m,n})$. Also, all of the equations for which the pixel $I(m, n)$ does not image the object should be excluded from the computation.)

Although we have described this algorithm for a single image $I(m, n)$, any number of images can obviously be used. The extra pixels from the other images are simply added in as additional constraints on the unknown coefficients λ_i in Equation (3).

3.3 Properties of the Eigen Light-Field Estimation Algorithm

The Eigen Light-Field Estimation Algorithm can be used to estimate a light-field from a collection of images. Once the light-field has been estimated, it can then, theoretically at least, be used to

render new images of the same object under different poses. See [26] for a related algorithm. In this section we show that if the objects used to create the eigen-space of light-fields all have the same shape as the object imaged to create the input to the algorithm, then this re-rendering process is in some sense "correct," assuming that all the objects are Lambertian. As a first step, we show that the eigen light-fields $E_i(\theta, \phi)$ capture the shape of the objects in the following sense:

Lemma 1 *If $\{L_i(\theta, \phi) \mid i = 1, \ldots, N\}$ is a collection of light-fields of Lambertian objects with the same shape, then all of the eigen light-fields $E_i(\theta, \phi)$ have the property that if (θ_1, ϕ_1) and (θ_2, ϕ_2) define two rays which image the same point on the surface of any of the objects then:*

$$E_i(\theta_1, \phi_1) \;=\; E_i(\theta_2, \phi_2) \qquad \forall i = 1 \ldots d. \tag{4}$$

Proof: The property in Equation (4) holds for all of the light-fields $\{L_i(\theta, \phi) | i = 1, \ldots, N\}$ used in the PCA because they are Lambertian. Hence, it also holds for any linear combination of the L_i. Therefore it holds for the eigen-vectors because they are linear combinations of the L_i. □

The property in Equation (4) also holds for all linear combinations of the eigen light-fields. It therefore holds for the light-field recovered in Equation (3) in the Light-Field Estimation Algorithm, assuming that the light-field from which the input image is derived lies in the eigen-space so that Theorem 9 applies. This means that the Light-Field Estimation Algorithm estimates the light-field in a way that is consistent with the object being Lambertian and of the appropriate shape:

Theorem 10 *Suppose $\{E_i(\theta, \phi) \mid i = 1, \ldots, d\}$ are the eigen light-fields of a set of Lambertian objects with the same shape and $I(m, n)$ is an image of another Lambertian object with the same shape. If the light-field from which $I(m, n)$ is derived lies in the light-field eigen-space, then the light-field recovered by the Light-Field Estimation Algorithm has the property that if $\theta_{m,n}, \phi_{m,n}$ is* any *pair of angles which image the same point in the scene as the pixel (m, n) then:*

$$I(m, n) \;=\; E(\theta_{m,n}, \phi_{m,n}). \tag{5}$$

where $E(\theta_{m,n}, \phi_{m,n})$ is the light-field estimated by the Light-Field Estimation Algorithm; i.e. the algorithm correctly re-renders the object under the Lambertian reflectance model.

Theorem 10 implies that the algorithm is acting reasonably in estimating the light-field, a task which is impossible from a single image without a prior model on the shape of the object. Here, the shape model is implicitly contained in the eigen light-fields. Theorem 10 assumes that all of the objects are approximately the same shape, but that is a common assumption for faces [21]. Even if there is some shape variation in faces, it is reasonable to assume that the eigen light-fields will capture this information. Theorem 10 also assumes that faces are Lambertian and that the light-field eigenspace accurately approximates any face light-field. The extent to which these assumptions are valid will be demonstrated by the empirical results obtained by our face recognition algorithm.

(Note: We are not proposing the Eigen Light-Field Estimation Algorithm as an algorithm for rendering across pose. It is only correct in a very idealized scenario. However, the fact that it is correct in this idealized scenario gives us confidence in its use for face recognition across pose.)

3.4 Application to Face Recognition Across Pose

The Eigen Light-Field Estimation Algorithm described above is somewhat abstract. In order to be able to use it for face recognition across pose we need to be able to do two things:

Vectorization: The input to a face recognition algorithm consists of a collection of images (possibly just one) captured from a variety of poses. The Eigen Light-Field Estimation Algorithm operates on light-field vectors (light-fields represented as vectors). Vectorization consists of converting the input images into a light-field vector (with missing elements, as appropriate.)

Classification: Given the eigen coefficients $\lambda_1 \ldots \lambda_d$ for a collection of gallery (training) faces and for a probe (test) face, we need to classify which gallery face is the most likely match.

We now describe each of these tasks in turn.

3.4.1 Vectorization by Normalization

Vectorization is the process of converting a collection of images of a face into a light-field vector. Before we can do this, we first have to decide how to discretize the light-field into pixels. Perhaps the most natural way to do this is to uniformly sample the light-field angles, θ and ϕ in the 2D case of Figure 2. This is not the only way to discretize the light-field. Any sampling, uniform or non-uniform, could be used. All that is needed is a way of specifying what is the allowed set of light-field pixels. For each such pixel, there is a corresponding index in the light-field vector; i.e. if the light-field is sampled at N pixels, the light-field vectors are N dimensional vectors.

We specify the set of light-field pixels in the following manner. We assume that there are only a finite set of poses $1, 2, \ldots P$ in which the face can occur. Each face image is first classified into the nearest pose. (Although this assumption is clearly an approximation, its validity is demonstrated by the empirical results in Section 3.5.3. In both the FERET [20] and PIE [23] databases, there is considerable variation in the pose of the faces. Although the subjects are asked to place their face in a fixed pose, they rarely do this perfectly. Both databases therefore contain considerable variation away from the finite set of poses. Since our algorithm performs well on both databases, the approximation of classifying faces into a finite set of poses is validated.)

Each pose $i = 1, \ldots, P$ is then allocated a fixed number of pixels N_i. The total number of pixels in a light-field vector is therefore $N = \sum_{i=1}^{P} N_i$. If we have images from pose 3 and 7, for example, we know $N_3 + N_7$ of the N pixels in the light-field vector. The remaining $N - N_3 - N_7$ are unknown, missing data. This vectorization process is illustrated in Figure 3.

We still need to specify how to sample the N_i pixels of a face in pose i. This process is analogous to that needed in appearance-based object recognition and usually performed by "normalization." In eigenfaces [25], the standard approach is to find the positions of several canonical points, typically the eyes and the nose, and to warp the input image onto a coordinate frame where these points are in fixed locations. The resulting image is then masked. To generalize eigenface normalization to eigen light-fields, we just need to define such a normalization for each pose.

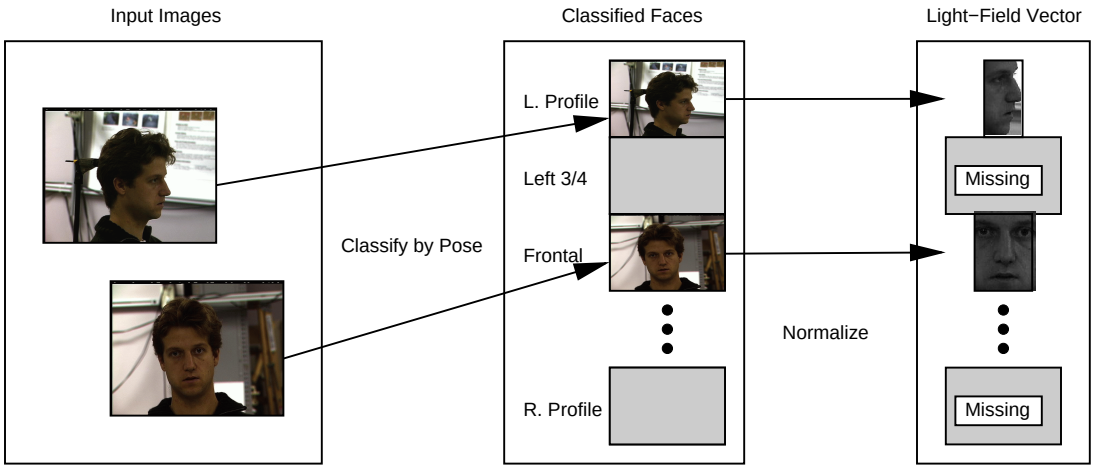

Figure 3: Vectorization by normalization. Vectorization is the process of converting a set of images of a face into a light-field vector. Vectorization is performed by first classifying each input image into one of a finite number of poses. For each pose, a normalization is then applied to convert the image into a sub-vector of the light-field vector. If poses are missing, the corresponding part of the light-field vector is missing.

In this paper we experimented with two different normalizations. The first one, illustrated in Figure 4(a) for three poses, is a simple one based on the location of the eyes and the nose. Just as in eigenfaces, we assume that the eye and nose locations are known, warp the face into a coordinate frame in which these canonical points are in a fixed location and finally crop the image with a (pose dependent) mask to yield the N_i pixels. For this simple 3-point normalization, the resulting masked images vary in size between 7200 and 12600 pixels.

The second normalization is more complex and is motivated by the success of Active Appearance Models [9]. This normalization is based on the location of a large number (39–54 depending on the pose) of points on the face. These canonical points are triangulated and the image warped with a piecewise affine warp onto a coordinate frame in which the canonical points are in fixed locations. See Figure 4(b) for an illustration of this multi-point normalization. The resulting masked images for this multi-point normalization vary in size between 20800 and 36000 pixels. Although currently the multi-point normalization is performed using hand-marked points, it could be performed by fitting an Active Appearance Model [9] and then using the implied canonical point locations. Further discussion of this way of automating our algorithm is contained in Section 5.2.

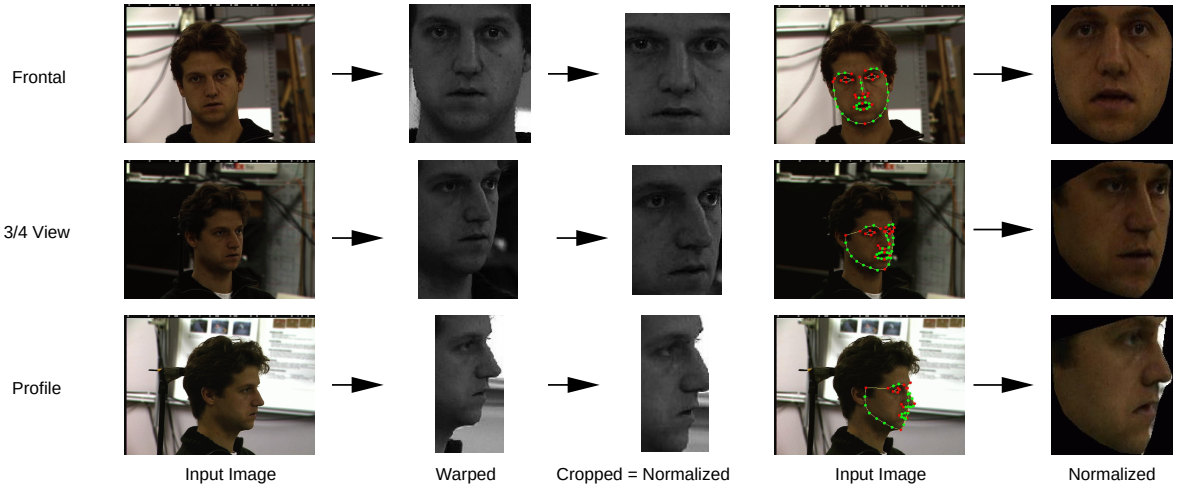

(a) 3-Point Normalization (b) Multi-Point Normalization

Figure 4: (a) The first, simpler normalization for three poses in the finite set in Figure 3, one frontal, one a 3/4 view, the final a full profile. Just as in eigenfaces, we assume that the eye and nose locations are known, warp the face into a coordinate frame in which these canonical points are in a fixed location and finally crop the image with a (pose dependent) mask. (b) The second, more complex normalization. In this case, a large number (39–54 depending on the pose) of points on the face are used to perform the normalization.

3.4.2 Classification using Nearest Neighbor

The Eigen Light-Field Estimation Algorithm outputs a vector of eigen coefficients $(\lambda_1, \ldots, \lambda_d)$. Given a set of gallery (training) faces, we obtain a corresponding set of vectors $(\lambda_1^{\mathrm{id}}, \ldots, \lambda_d^{\mathrm{id}})$, where id is an index over the set of gallery faces. Similarly, given a probe (or test) face, we obtain a vector $(\lambda_1, \ldots, \lambda_d)$ of eigen coefficients for that face. To complete the face recognition algorithm we need an algorithm which classifies $(\lambda_1, \ldots, \lambda_d)$ with the index id which is the most likely match. Many different classification algorithms could be used for this task. For simplicity, we use the nearest neighbor algorithm which classifies the vector $(\lambda_1, \ldots, \lambda_d)$ with the index:

$$\arg\min_{\mathrm{id}} \mathrm{dist}\left((\lambda_1, \ldots, \lambda_d), (\lambda_1^{\mathrm{id}}, \ldots, \lambda_d^{\mathrm{id}})\right) = \arg\min_{\mathrm{id}} \sum_{i=1}^{d} \left(\lambda_i - \lambda_i^{\mathrm{id}}\right)^2. \quad (6)$$

All of the results reported in this paper use the Euclidean distance in Equation (6). Alternative distance functions, such as the Mahalanobis distance, could be used instead if so desired.

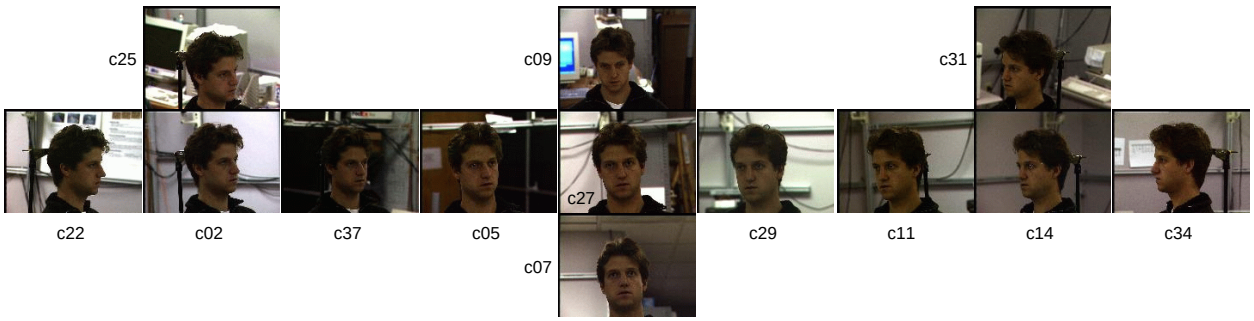

Figure 5: An illustration of the pose variation in the CMU PIE database [23]. The pose varies from full right profile (c02) to full frontal (c27) and on to full left profile (c34). The 9 cameras in the horizontal sweep are each separated by about $22.5°$. The 4 other cameras include 1 above (c09) and 1 below (c07) the central camera, and 2 in the corners of the room (c25 and c31), typical locations for surveillance cameras.

3.5 Experimental Results

3.5.1 Databases

We used two databases in our face recognition across pose experiments, the CMU Pose, Illumination, and Expression (PIE) database [23] and the FERET database [20]. Each of these databases contains substantial pose variation. In the pose subset of the CMU PIE database (see Figure 5), the 68 subjects are imaged simultaneously under 13 different poses totaling 884 images. In the FERET database, the subjects are imaged non-simultaneously in 9 different poses. See Figure 6 for an example. We used 75 subjects from the FERET pose subset giving 675 images in total. (In both cases, we used greyscale images even if the database actually contains color images.)

3.5.2 Selecting the Gallery, Probe, and Generic Training Data

In each of our experiments we divided the database(s) into three disjoint subsets:

Generic Training Data: Many face recognition algorithms such as eigenfaces, and including our algorithm, require "generic training data" to build a generic face model. In eigenfaces, for

bb bc bd be ba bf bg bh bi

Figure 6: An illustration of the pose variation in the FERET database [20]. The poses of the 9 images vary from $+60^\circ$ (bb) to full frontal (ba) and on to -60° (bi). Overall, the variation in pose is somewhat less than in the CMU PIE database. See Figure 5 for an illustration of the pose variation in the PIE database.

example, generic training data is needed to compute the eigenspace. Similarly, in our algorithm generic data is needed to construct the eigen light-field.

Gallery: The gallery is the set of "training" images of the people to be recognized; i.e. the images given to the algorithm as examples of each person that might need to be recognized.

Probe: The probe set contains the "test" images; i.e. the examples of images to be presented to the system that should be classified with the identity of the person in the image.

The division into these three subsets is performed as follows. First we randomly select half of the subjects as generic training data. The images of the remaining subjects are used for the gallery and probe. There is never any overlap between the generic training data and the gallery and probe. For the PIE database we randomly select 34 subjects for the generic training data. For the FERET database we randomly select 38 subjects for the generic training data.

After the generic training data has been removed, the remainder of the database(s) is divided into probe and gallery sets based on the pose of the images. For example, we might set the gallery to be the frontal images and the probe set to be the left profiles. In this case, we evaluate how well our algorithm is able to recognize people from their profiles given that the algorithm has only seen them from the front. In the experiments described below we choose the gallery and probe poses in various different ways. The gallery and probe are always completely disjoint however.

3.5.3 Experiment 1: Comparison with Other Algorithms

We first conducted an experiment to compare our algorithm with two others. In particular we compared our algorithm with eigenfaces [25] and FaceIt, the commercial face recognition system from Identix (formerly Visionics). Eigenfaces is the defacto baseline standard by which face recognition algorithms are compared. FaceIt finished top overall in the Face Recognition Vendor Test 2000 [7].

We first performed a comparison using the PIE database [23]. After randomly selecting the generic training data, we selected the gallery pose as one of the 13 PIE poses and the probe pose as any other of the remaining 12 PIE poses. For each disjoint pair of gallery and probe poses, we compute the average recognition rate over all subjects in the probe and gallery sets. The details of the results are included in Figures 7–8 and a summary is included in Table 3.

In Figure 7 we plot color-coded 13×13 "confusion matrices" of the results. The row denotes the pose of the gallery, the column the pose of the probe, and the displayed intensity the average recognition rate. A lighter color denotes a higher recognition rate. (On the diagonals the gallery and probe images are the same and so all three algorithms obtain a 100% recognition rate.) Eigen light-fields performs far better than the other algorithms, as is witnessed by the lighter color of Figures 7(a–b) compared to Figures 7(c–d). Note how eigen light-fields is far better able to generalize across wide variations in pose, and in particular to and from near profile views.

Several "cross-sections" through the confusion matrices in Figure 7 are shown in Figure 8. In each cross-section, we fix the pose of the gallery images and vary the pose of the probe image. In each graph we plot four curves, one for eigenfaces, one for FaceIt, one for eigen light-fields with the 3-point normalization, and one for eigen light-fields with the multi-point normalization. As can be seen, eigen light-fields outperforms the other two algorithms. In particular, it is better able to recognize the face when the gallery and probe poses are very different. This is witnessed by the eigen light-field curves in Figure 8 being higher at the extremities of the probe pose range.

The results in Figures 7 and 8 are summarized in Table 3. In this table we include the average recognition rate computed over all disjoint gallery-probe poses. As can be seen, eigen

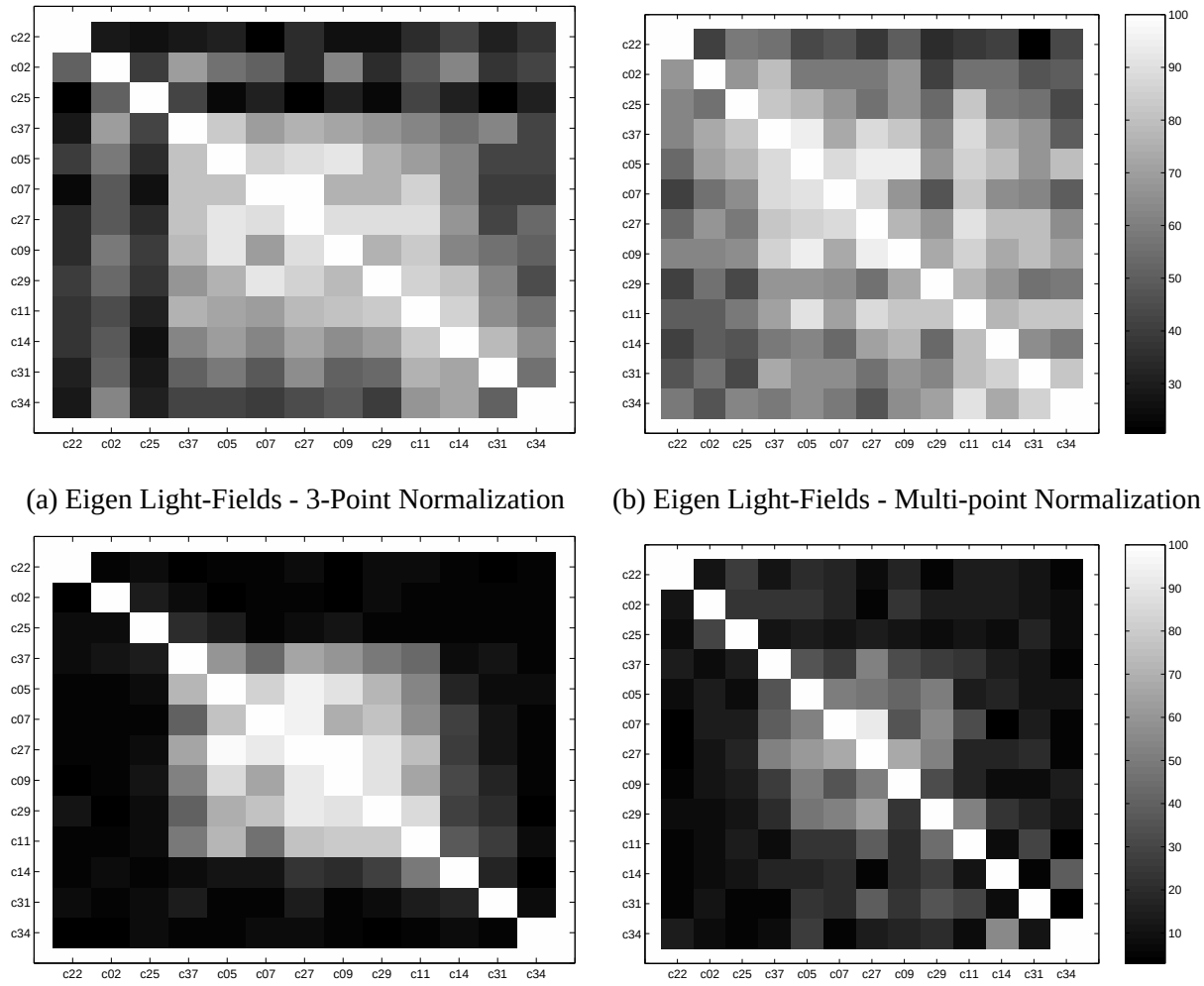

(a) Eigen Light-Fields - 3-Point Normalization

(b) Eigen Light-Fields - Multi-point Normalization

(c) FaceIt

(d) Eigenfaces

Figure 7: A comparison with FaceIt and eigenfaces for face recognition across pose on the PIE database. For each pair of gallery and probe poses, we plot the color-coded average recognition rate. The fact that the images in (a) and (b) are lighter in color than those in (c) and (d) implies that our algorithm performs better.

light-fields outperforms both the standard eigenfaces algorithm and the commercial FaceIt system.

We next performed a similar comparison using the FERET database [20]. Just as with the PIE database, we selected the gallery pose as one of the 9 FERET poses and the probe pose as any other of the remaining 8 FERET poses. For each disjoint pair of gallery and probe poses, we compute the average recognition rate over all subjects in the probe and gallery sets, and then average the results. The results are very similar to those for the PIE database and are summarized

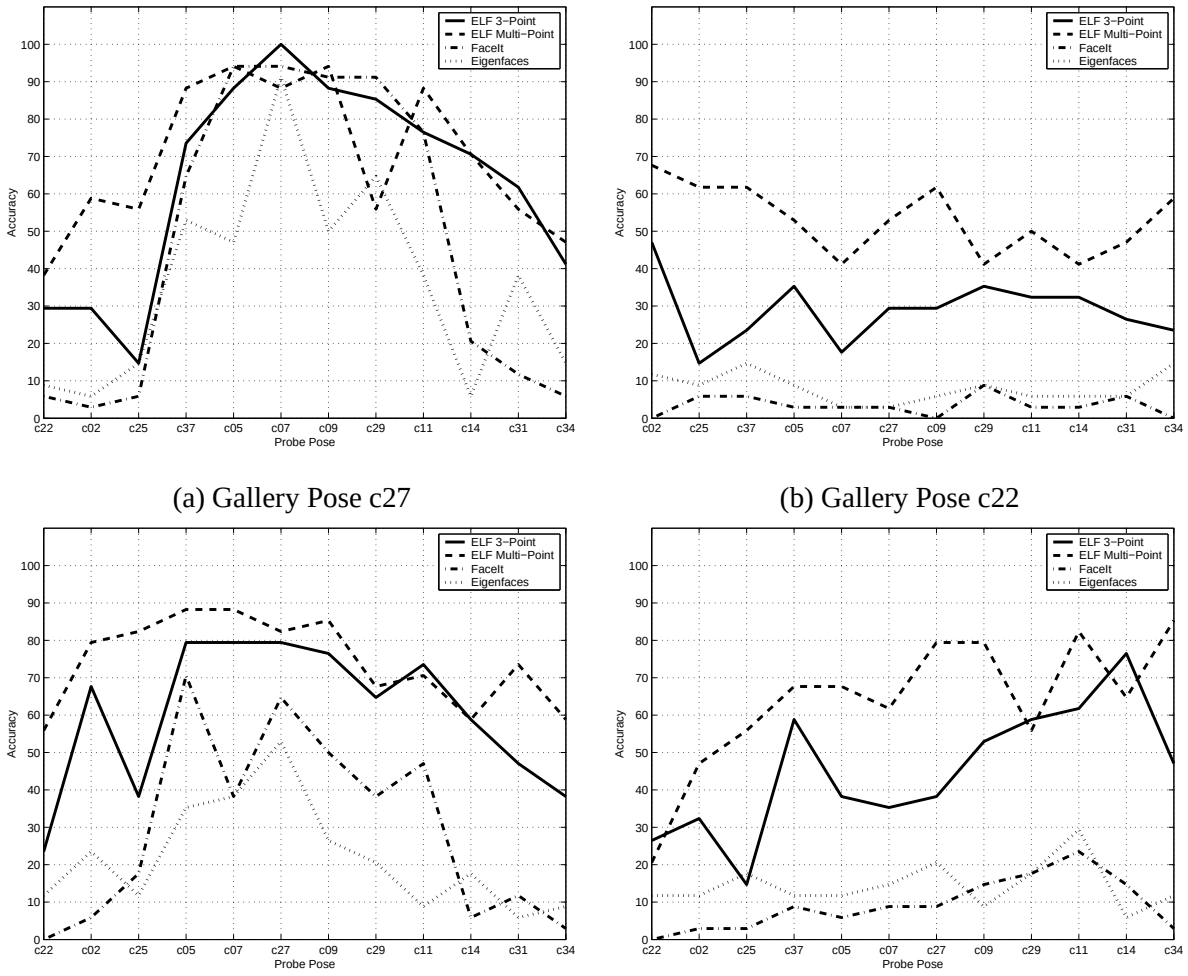

(a) Gallery Pose c27

(b) Gallery Pose c22

(c) Gallery Pose c37

(d) Gallery Pose c31

Figure 8: Several "cross-sections" through the confusion matrices in Figure 7. In each figure we fix the pose of the gallery and only vary the pose of the probe. We plot four curves, one each for eigen light-fields with the 3-point normalization, eigen light-fields with the multi-point normalization, eigenfaces, and FaceIt. The performance of eigen light-fields is superior to that for the other two algorithms, particularly when the pose of the gallery and probe are radically different. Eigen light-fields recognizes faces better across pose.

in Table 4. Again, eigen light-fields performs significantly better than both FaceIt and eigenfaces.

Overall, the performance improvement of eigen light-fields over the other two algorithms is more significant on the PIE database than on the FERET database. This is because the PIE database contains more variation in pose than the FERET database. See Figures 5 and 6.

Table 3: A comparison of eigen light-fields with FaceIt and eigenfaces for face recognition across pose on the PIE database. The table contains the average recognition rate computed across all disjoint pairs of gallery and probe poses; i.e. this table summarizes the average performance in Figure 7.

	Eigenfaces	FaceIt	Eigen Light-Fields 3-Point Normalization	Eigen Light-Fields Multi-Point Normalization
Average Recognition Rate	16.6%	24.3%	52.5%	66.3%

Table 4: A comparison of eigen light-fields with FaceIt and eigenfaces for face recognition across pose on the FERET database. The table contains the average recognition rate computed across all disjoint pairs of gallery and probe poses. Again, eigen light-fields outperforms both eigenfaces and FaceIt.

	Eigenfaces	FaceIt	Eigen Light-Fields 3-Point Normalization
Average Recognition Rate	53.2%	70.8%	80.3%

3.5.4 Experiment 2: Improvement with the Number of Input Images

So far we have assumed that just a single gallery and probe image are available to the algorithm. What happens if more gallery and/or probe images are available? In Experiment 2 we investigate the performance of eigen light-fields with different numbers of images using the PIE database. To compute the recognition rate with n gallery images, we select every possible set of n gallery poses and 1 probe pose. In total this amounts to $13 \times 12 \times \ldots (13-n)/n!$ different combinations of poses. We then compute the average recognition rate for each such combination and average the results. We plot the overall average recognition rate against the number of gallery images in Figure 9(a). As can be seen, eigen light-fields is able to estimate a more accurate light-field using more gallery images and thereby obtain a higher recognition rate.

Eigen light-fields can also take advantage of more than one probe image. We therefore repeated Experiment 2 but reversed the roles of the gallery and probe. The results are shown in Figure 9(b). Again the performance increases with the number of probe images, however the

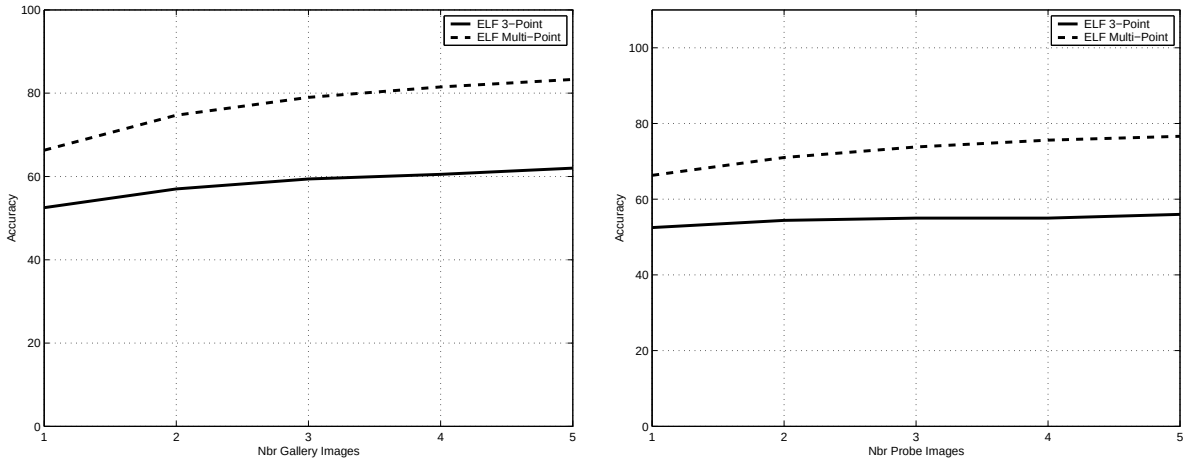

(a) Varying the Number of Gallery Images (b) Varying the Number of Probe Images

Figure 9: (a) The improvement in the performance of our algorithm with increasing numbers of gallery images. Using the additional images, eigen light-fields is able to estimate the light-fields more accurately and thereby obtains a higher recognition rate. (b) The performance of eigen light-fields also improves with the number of probe images. The performance increase is greater with increased numbers of gallery images because the accuracy of the light-field of every gallery subject is improved. On the other hand, with more probe images, the accuracy of just the one probe subject is improved.

benefit of using multiple probe images is not as much as the benefit of using multiple gallery images. With multiple gallery images the accuracy of the light-field of every subject in the gallery is improved. With more probe images, the accuracy of the light-field of just the single probe subject is improved.

3.5.5 Experiment 3: Matching Sub-Images

We just illustrated how the performance of eigen light-fields improves if more gallery and/or probe images are available. Eigen light-fields can use any subset of the light-field. In particular, it does not even need a complete image. To validate this property, we ran the following experiment. We repeated Experiment 1, but for each pair of gallery and probe poses, we randomly selected a certain percentage of the pixels in the masked image. We then compute the average recognition rate just using this subset of the pixels. This process is repeated for 100 random samples of pixels and the results averaged. The results are plot in Figure 10 for a variety of pixel percentages ranging from

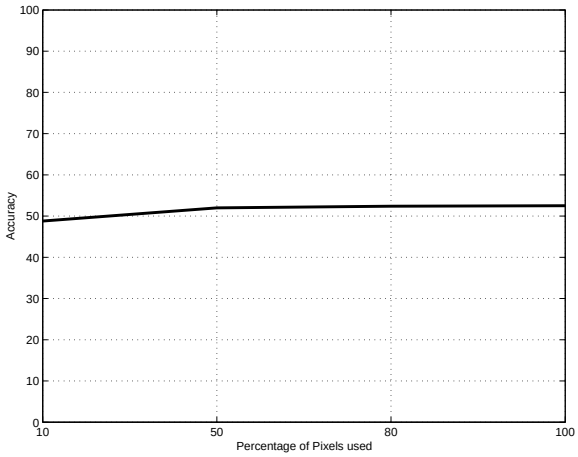

Figure 10: The performance of eigen light-fields with a subset of the images using the 3-point normalization and the PIE database. The average recognition rate is plot against the percentage of pixels in the probe and gallery images. A subset of the images can be used without any significant reduction in the recognition rate.

10% to 100% (the complete image). These results were obtained using the 3-point normalization and so the performance with 100% is 52.5%, as per Table 3. The figure clearly demonstrates that a subset of the images can be used without any significant reduction in the recognition rate.

3.5.6 Experiment 4: Division of the Input Images between Gallery and Probe

In Experiment 2 we examined the benefits of using more than one gallery or probe image. Suppose that n gallery and probe images are available in total. Is it better to use $n-1$ gallery and 1 probe images or $n/2$ gallery and $n/2$ probe images? In order to answer this question, we conducted Experiment 4. Given n images, we generated every possible combination of $n-1$ gallery images and 1 probe image (as in Experiment 2) and every possible combination of $n/2$ gallery images and $n/2$ probe images. We then computed the average recognition rate for each case. Similarly we switched the roles of gallery and probe. The results are shown in Figure 11. The conclusion is clear. It is better to divide the images equally between gallery and probe rather than asymmetrically.

One possible conclusion from this result is that adding more that one image to each of the probe and gallery allows a better estimate of the light-field. Having two more accurate estimates results in better performance than having one very accurate estimate and one not so accurate

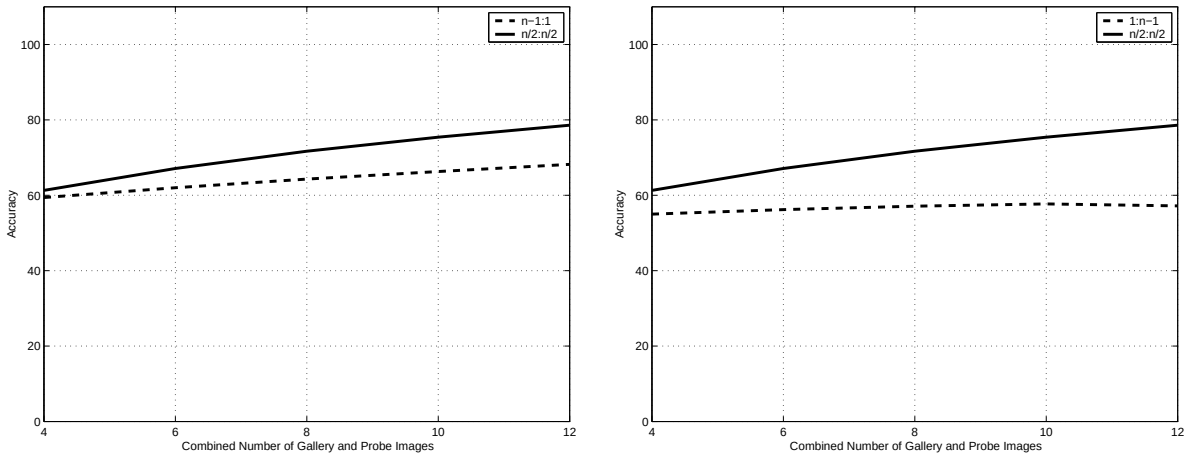

(a) $n-1$ gallery, 1 probe vs. $n/2$ of each (b) 1 gallery, $n-1$ probe vs. $n/2$ of each

Figure 11: (a) The performance of using $n-1$ gallery images and 1 probe image versus using $n/2$ of each. The empirical evidence suggests to split up the images evenly into gallery and probe. (b) The performance of using 1 gallery image and $n-1$ probe images versus using $n/2$ of each. Again splitting up the images evenly achieves higher recognition rates. Having two more accurate estimates of the light-fields results in better performance than having one very accurate estimate and one not so accurate estimate.

estimate.

4 Fisher Light-Fields for FR Across Pose and Illumination

After pose variation the next most significant factor affecting the appearance of faces is illumination. In many face recognition application scenarios both the *pose* and *illumination* of the probe and gallery images may be different. The gallery images may be two frontal and profile "mug-shots" captured in well controlled lighting. The probe may be a single 3/4 view captured from a surveillance camera in the corner of a room with strong overhead lighting.

Whereas face recognition across pose has received very little attention in the literature, a number of approaches have been proposed for face recognition across illumination. Examples include, discarding the first 3 eigen-vectors in eigenfaces, using discriminant analysis [3], and using image illumination cones [5]. Some of these approaches, for example image illumination cones [5], require multiple gallery images captured with significant illumination variation. We would

like an algorithm that can operate with just a single gallery and probe image. We chose to combine Fisherfaces [3] with eigen light-fields [13] to obtain Fisher light-fields [14]. After describing how these two techniques can be combined to give an algorithm for face recognition across pose and illumination, we complete this section by presenting experimental results in Section 4.2.

4.1 Fisher Light-Fields

Suppose now that we are given a set of light-fields $L_{i,j}(\theta, \phi)$, $i = 1, \ldots, N, j = 1, \ldots, M$ where each of N objects O_i is imaged under M different illumination conditions. We could proceed as described above and perform Principal Component Analysis on the whole set of $N \times M$ light-fields. This approach ignores object affiliations and effectively re-indexes the set of light-fields as $L_k, k = 1, \ldots, N \times M$. Define the *total scatter* matrix S_T as:

$$S_T = \sum_{k=1}^{N \times M} (L_k(\theta, \phi) - \mu)(L_k(\theta, \phi) - \mu)^T$$

where μ is the mean of the complete light-field set. PCA determines the orthogonal projection Φ:

$$y_k = \Phi^T L_k(\theta, \phi), k = 1, \ldots, N \times M \tag{7}$$

that maximizes the determinant of the total scatter matrix of the projected samples $y_1, \ldots, y_{N \times M}$:

$$\Phi_{opt} = \arg\max_{\Phi} \mid \Phi^T S_T \Phi \mid .$$

This scatter stems from both *inter-class* variations between the objects, as well as from *intra-class* variation within the object classes. In practice, most of the scatter is due to illumination changes. Consequently PCA encodes the illumination variations and fails to discriminate well between object classes. An alternative approach is Fisher's Linear Discriminant [10], also known as Linear Discriminant Analysis [27]. Fisher's Linear Discriminant uses the available class information to compute a projection better suited for discrimination tasks.

Define the *within-class* scatter matrix S_W as:

$$S_W = \sum_{i=1}^{N} \sum_{j=1}^{M} (L_{i,j}(\theta, \phi) - \mu_i)(L_{i,j}(\theta, \phi) - \mu_i)^T$$

where μ_i is the mean of class i. Furthermore define the *between-class* scatter matrix S_B as

$$S_B = \sum_{i=1}^{N} N_i(\mu_i - \mu)(\mu_i - \mu)^T$$

where N_i refers to the number of samples in class i. Fisher's Linear Discriminant computes the projection Ψ that maximizes the ratio:

$$\Psi_{opt} = \arg\max_{\Psi} \frac{\mid \Psi^T S_B \Psi \mid}{\mid \Psi^T S_W \Psi \mid}.$$

The optimal projection Ψ_{opt} is found by solving the generalized eigenvalue problem:

$$S_B \Psi = \lambda S_W \Psi.$$

Due to the structure of the data, the within-class scatter matrix S_W is always singular. We overcome this problem by first using PCA to reduce the dimension and then applying Fisher's Linear Discriminant [3] in the lower dimensional PCA subspace where the within-class scatter matrix S_W is non-singular. The overall projection is given by $W_{opt}^T = \Psi_{opt}^T \Phi_{opt}^T$. Analogously to the Eigen Light-Field Estimation Algorithm, with Fisher light-fields we find the least squares solution to:

$$L(\theta, \phi) - \sum_{i=1}^{m} \lambda_i W_i(\theta, \phi) = 0 \tag{8}$$

where $W_i, i = 1, \ldots, m$ are the generalized eigenvectors of S_B and S_W. Note that there are at most $N - 1$ nonzero generalized eigenvectors. This extension of eigen light-fields to Fisher light-fields mirrors the step from eigenfaces to Fisherfaces as proposed in [3].

4.2 Experimental Results

4.2.1 Databases

For our face recognition across pose and illumination experiments, we used the pose and illumination subset of the PIE database [23]. In this subset, 68 subjects are imaged under 13 different poses and 21 illumination conditions. Many of the illumination directions introduce fairly subtle

Figure 12: An illustration of the pose and illumination variation in the CMU PIE database [23]. The pose varies from full right profile (c22) to full frontal (c27) and on to full left profile (c34). Similarly, the illumination (flash) locations span the full range from right profile (f16) to left profile (f02).

variations in appearance and so we selected 12 of the 21 illumination conditions which span the set widely. The set of 13 pose variations and 12 illumination variations are illustrated for one subject in Figure 12. In total we used $68 \times 13 \times 12 = 10,6084$ images in the experiments. Although the PIE database contains color images, all of the experiments in this paper use greyscale images.

4.2.2 Selecting the Gallery, Probe, and Generic Training Data

We select the generic training data just as in Section 3.5.2. We randomly select 34 subjects of the PIE database for the generic training data and then remove this data from the experiments. There are then a variety of ways of selecting the gallery and probe images from the remaining data:

Same Pose, Different Illumination: The gallery and probe poses are the same. The gallery and probe illuminations are different. This scenario is like traditional face recognition across illumination, but is performed separately for each pose.

Different Pose, Same Illumination: The gallery and probe poses are different. The gallery and probe illuminations are the same. This scenario is like traditional face recognition across pose, but is performed separately for each possible illumination.

Different Pose, Different Illumination: Both the pose and illumination of the probe and gallery are different. This is the hardest and most general scenario.

4.2.3 Experiment 5: Comparison with Other Algorithms

We compare our algorithms with FaceIt under these three scenarios. In all cases we generate every possible test scenario and then average the results. For “same pose, different illumination”, for example, we consider every possible pose. We then generate every pair of disjoint probe and gallery illumination conditions. We then compute the average recognition rate for each such case. For example, we might compare probe pose c27, illumination f11 against gallery pose c27, illumination f21. We then average over every pose and every pair of distinct illumination conditions.

Table 5: A comparison of the performance of eigen light-fields and Fisher light-fields with FaceIt on three different face recognition across pose and illumination scenarios. In all three cases, eigen light-fields and Fisher light-fields outperform FaceIt by a large margin.

	Eigen Light-Fields	Fisher Light-Fields	FaceIt
Same pose, Different illumination	-	81.1	41.6
Different pose, Same illumination	72.9	-	25.8
Different pose, Different illumination	-	36.0	18.1

The results are included in Table 5. For "same-pose, different illumination," the task is essentially face recognition across illumination separately for each pose. In this case, it makes little sense to try eigen light-fields since we know how poorly eigenfaces performs with illumination variation. Fisher light-fields becomes Fisher faces for each pose which empirically we find outperforms FaceIt. Example illumination "confusion matrices" are included for two poses in Figure 13.

For "different pose, same illumination," the task reduces to face recognition across pose but for a variety of different illumination conditions. In this case there is no intra-class variation and so it makes little sense to apply Fisher light-fields. This experiment is the same as Experiment 1 but the results are averaged over every possible illumination condition. As we found for Experiment 1, eigen light-fields outperforms FaceIt by a large amount.

Finally, in the "different pose, different illumination" task both algorithms perform fairly poorly. The task is very difficult, however, as can be seen in Figure 12. If the pose and illumination are both extreme, almost none of the face is visible. Since this case might occur in either the probe or the gallery, the chances that such a difficult case occurs is quite large. Although more work is needed on this task, note that Fisher light-fields still outperforms FaceIt by a large amount.

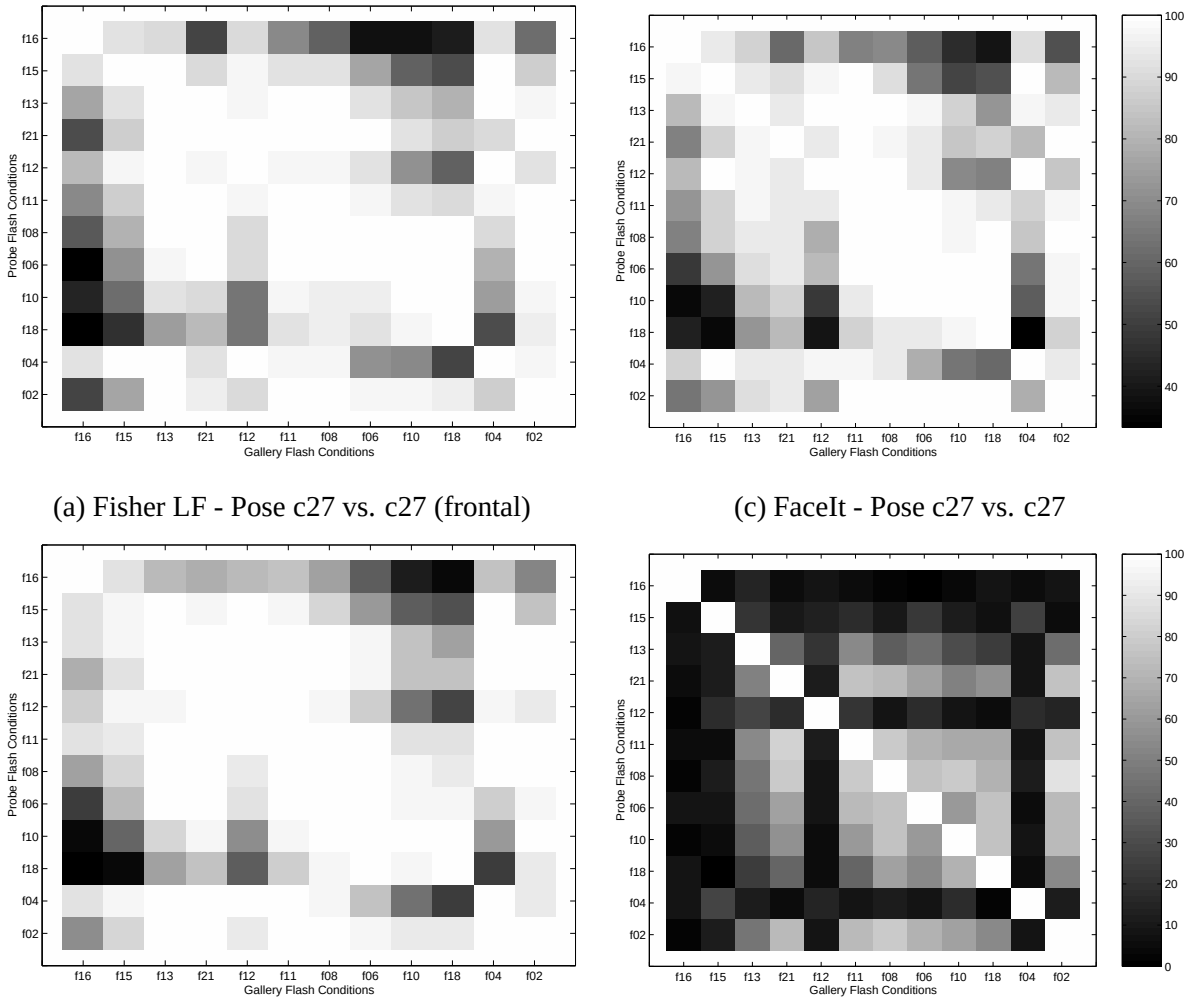

(a) Fisher LF - Pose c27 vs. c27 (frontal)

(c) FaceIt - Pose c27 vs. c27

(b) Fisher LF - Pose c37 vs. c37 (right $3/4$)

(d) FaceIt - Pose c37 vs. c37

Figure 13: Example "confusion matrices" for the "same-pose, different illumination" task. For a given pose, and a pair of distinct probe and gallery illumination conditions, we color-code the average recognition rate. The superior performance of Fisher light-fields is witnessed by the lighter color of (a–b) over (c–d).

5 Conclusion

5.1 Summary

Appearance-based object recognition uses pixels or measurements of light in the scene as its features. In the ultimate limit, the set of all such measurements is the plenoptic function or light-field. In this paper we have explored appearance-based object recognition from light-fields. We first

analyzed the theoretical distinguishability of objects from their images and light-fields. We presented a number of results which show that theoretically objects can be distinguishable from their light-fields in cases that they are ambiguous from just a single image. This theoretical analysis motivates trying to build appearance-based object recognition algorithms that use as much of the light-field as is available, be it a single image, a pair of images, or multiple images.

In the second half of this paper we proposed an appearance-based algorithm for face recognition across pose based on an algorithm to estimate the (eigen) light-field from a collection of images. This algorithm can use any number of gallery images captured form arbitrary poses and any number of probe images also captured from arbitrary poses. The gallery and probe poses do not need to overlap, and any number of gallery and probe images can be used. We showed that our algorithm can reliably recognize faces across pose and also take advantage of the additional information contained in widely separated views to improve recognition performance if more than one gallery or probe image is available. We extended our algorithm to recognize faces across both pose and illumination simultaneously by generalizing eigen light-fields [13] to Fisher light-fields [14], analogously to how eigen faces [25] can be generalized to Fisherfaces [3].

5.2 Limitations and Future Work: Normalization

Appearance-based object recognition algorithms require that the images be aligned. In eigenfaces [25] the images are normally warped so that the eyes, and perhaps the nose, are in canonical locations. Why is this alignment needed? It is needed to make sure that the features used in the training phase match up with the features used in the testing phase. As we have pointed out, the features used in appearance-based algorithms are the radiances of light along certain rays in space. For such algorithms to be meaningful, the light radiated from the cheek of one person, say, must correspond to the same features as the light radiated from the cheek of another person.

With 2D images of frontal faces a simple translation (or perhaps an affine warp) is enough to register faces. With light-fields of 3D objects, the registration is a 6 DOF rigid transformation

(rotation plus translation) in the 3D world (perhaps followed by a correction for the intrinsics of the camera.) Although performing such a registration is more difficult in 3D, in essence it is performing the same function as the simple translation or affine warp in 2D, namely to ensure that the same light rays correspond to the same pixels (features.)

In this paper we used two different normalizations based on manually marked locations of the eyes and nose, etc, combined with the known pose of the face, to perform this registration. See Section 3.4.1 for the details. The essence of this step is to convert the input image into the light-field coordinate frame in a way that the same light rays for each subject (training and testing) get mapped to the same pixels in the light-field. At present our algorithm is somewhat ad-hoc and requires user input in the form of feature point location. We are currently working on using "active appearance models" [9] to perform this registration in a more principled and automated way.

Acknowledgements

Much of Section 3 first appeared in [13] and much of Section 4 in [14]. We would like to thank Terence Sim and Takeo Kanade for preliminary discussions on the light-field estimation algorithm and the reviewers of [13] and [14] for their feedback. The research described in this paper was supported by U.S. Office of Naval Research contract N00014-00-1-0915. Portions of the research in this paper use the FERET database of facial images collected under the FERET program.

References

[1] E.H. Adelson and J. Bergen. The plenoptic function and elements of early vision. In Landy and Movshon, editors, *Computational Models of Visual Processing*. MIT Press, 1991.

[2] S. Baker, T. Sim, and T. Kanade. When is the shape of a scene unique given its light-field: A fundamental theorem of 3D vision? *IEEE Transaction on Pattern Analysis and Machine Intelligence*, 2002. (Accepted for publication).

[3] P.N. Belhumeur, J. Hespanha, and D.J. Kriegman. Eigenfaces vs. Fisherfaces: Recognition using class specific linear projection. *IEEE Transactions on Pattern Analysis and Machine Intelligence*, 19(7):711–720, 1997.

[4] P.N. Belhumeur and D.W. Jacobs. Comparing images under variable illumination. In *Proceedings of the IEEE Conference on Computer Vision and Pattern Recognition*, 1998.

[5] P.N. Belhumeur and D.J. Kriegman. What is the set of images of an object under all possible lighting conditions? *International Journal of Computer Vision*, 28(3):1–16, 1998.

[6] M. Black and A. Jepson. Eigen-tracking: Robust matching and tracking of articulated objects using a view-based representation. *International Journal of Computer Vision*, 36(2):101–130, 1998.

[7] D.M. Blackburn, M. Bone, and P.J. Phillips. Facial recognition vendor test 2000: Evaluation report, 2000.

[8] V. Blanz, S. Romdhani, and T. Vetter. Face identification across different poses and illumination with a 3D morphable model. In *Proceedings of the Fifth International Conference on Face and Gesture Recognition*, 2002.

[9] T.F. Cootes, G.J. Edwards, and C.J. Taylor. Active appearance models. *IEEE Transactions on Pattern Analysis and Machine Intelligence*, 23(6):681–685, 2001.

[10] K. Fukunaga. *Introduction to statistical pattern recognition*. Academic Press, 1990.

[11] A. Georghiades, P.N. Belhumeur, and D. Kriegman. From few to many: Generative models for recognition under variable pose and illumination. In *Proceedings of the Fourth International Conference on Face and Gesture Recognition*, 2000.

[12] S. J. Gortler, R. Grzeszczuk, R. Szeliski, and M. F. Cohen. The lumigraph. In *Computer Graphics Proceedings, Annual Conference Series (SIGGRAPH)*, 1996.

[13] R. Gross, I. Matthews, and S. Baker. Eigen light-fields and face recognition across pose. In *Proceedings of the Fifth International Conference on Face and Gesture Recognition*, 2002.

[14] R. Gross, I. Matthews, and S. Baker. Fisher light-fields for face recognition across pose and illumination. In *Proceedings of the German Symposium on Pattern Recognition (DAGM)*, 2002.

[15] A. Leonardis and H. Bischof. Dealing with occlusions in the eigenspace approach. In *Proceedings of the IEEE Conference on Computer Vision and Pattern Recognition*, 1996.

[16] M. Levoy and M. Hanrahan. Light field rendering. In *Computer Graphics Proceedings, Annual Conference Series (SIGGRAPH)*, 1996.

[17] H. Murase and S.K. Nayar. Visual learning and recognition of 3-D objects from appearance. *International Journal of Computer Vision*, 14:5–24, 1995.

[18] S.G. Narasimhan and S.K. Nayar. Chromatic framework for vision in bad weather. In *Proceedings of the IEEE Conference on Computer Vision and Pattern Recognition*, 2000.

[19] A.P. Pentland, B. Moghaddam, and T. Starner. View-based and modular eigenspaces for face recognition. In *Proceedings of the IEEE Conference on Computer Vision and Pattern Recognition*, 1994.

[20] P. J. Phillips, H. Wechsler, J. Huang, and P. Rauss. The FERET database and evaluation procedure for face recognition algorithms. *Image and Vision Computing*, 16(5):295–306, 1998.

[21] T. Riklin-Raviv and A. Shashua. The Quotient image: Class based recognition and synthesis under varying illumination. In *Proceedings of the IEEE Conference on Computer Vision and Pattern Recognition*, 1999.

[22] S. Romdhani, V. Blanz, and T. Vetter. Face identification by matching a 3D morphable model using linear shape and texture error functions. In *Proceedings of the European Conference on Computer Vision*, 2002.

[23] T. Sim, S. Baker, and M. Bsat. The CMU pose, illumination, and expression (PIE) database. In *Proceedings of the Fifth International Conference on Face and Gesture Recognition*, 2002.

[24] L. Sirovich and M. Kirby. Low-dimensional procedure for the characterization of human faces. *Journal of the Optical Society of America*, 4(3):519–524, 1987.

[25] M. Turk and A. Pentland. Face recognition using eigenfaces. In *Proceedings of the IEEE Conference on Computer Vision and Pattern Recognition*, 1991.

[26] T. Vetter and T. Poggio. Linear object classes and image synthesis from a single example image. *IEEE Transactions on Pattern Analysis and Machine Intelligence*, 19(7):733–741, 1997.

[27] W. Zhao, A. Krishnaswamy, R. Chellappa, D.L. Swets, and J. Weng. Discriminant analysis of principal components for face recognition. In H. Wechsler, P.J. Phillips, V. Bruce, and T. Huang, editors, *Face Recognition: From Theory to Applications*. Springer Verlag, 1998.